Regular Article

Devitrification of ultrafast laser plasma produced metastable glass layer

Jayakrishnan Chandrappan [a,*], Vishal Khetan [b], Michael Ward [c], Matthew Murray [a], Gin Jose [a]

[a] School of chemical and process engineering, University of Leeds, LS2 9JT, UK
[b] School of mechanical engineering, University of Leeds, LS2 9JT, UK
[c] Leeds electron microscopy and spectroscopy centre, University of Leeds, LS2 9JT, UK

ARTICLE INFO

ABSTRACT

Erbium-doped tellurite modified silica (EDTS) is a newly formulated silicate glass that has the potential to realize on-chip optical amplifiers. The devitrification process of EDTS layer on host silica glass has been studied in the temperature range 300 °C–1000 °C. In-situ high-temperature X-ray diffraction, selective area electron diffraction and high-resolution transmission electron microscopy revealed the amorphous phase of EDTS as-fabricated up to 600 °C and rapid irreversible crystalline phase developments above 600 °C, contrasting the host silica. Distinct structural evolutions of EDTS with the variation in temperature were observed, including a complete evaporation of TeO_2 at 800 °C from the matrix.

Erbium doped silicates are the sole material platforms for manufacturing erbium-doped fiber amplifiers (EDFA) that are efficient optical signal boosters used in a fiber optic communication systems [1–5]. Generally, the amount of erbium and its homogeneous distribution in silica determine the magnitude of light amplification, known as the optical gain [6,7]. The optical gain is high with higher erbium concentration in silica. However, due to the chemical compositional limitations of silica, even a moderate concentration of erbium (>0.1 at.%) in silica leads to clustering that degrades the signal strength [6,8,9]. Therefore, minimally doped long lengths (>5 m) of EDFAs are maintained in current optical communication networks, which cannot be incorporated in the new generation compact integrated circuits that combine both optical and electrical components on a single substrate such as silicon photonics [10–15].

To realize compact optical amplifiers, we have developed a prospective material platform - erbium-doped tellurite modified silicate (EDTS) - by overcoming the fundamental limitations of erbium doping in silica utilizing a femtosecond (fs) laser plasma assisted novel process [16–18]. In this process, a tellurite glass target of composition (80-x)TeO_2-10ZnO-10Na_2O-xEr_2O_3 (TZNE) was prepared using standard glass melt-quenching process and then ablated using a fs-laser, inside a vacuum chamber. The highly energetic fs-laser generated plasma (ions and nano-particulates) [19], in 70 mTorr of oxygen within the vacuum chamber reacts with the host silica glass kept at a temperature of 700 °C and 70 mm above the target glass. These complex interfacial reactions between the TZNE plasma and the silica substrate cause the gradual dissolution of silica into the tellurite network to form the EDTS [16,18]. Such a homogeneous mixing of immiscible systems

(tellurite and silica) and glass formation cannot be achieved through any existing glass fabrication process. The optically transparent EDTS could contain record high levels of Er^{3+} ions [18] and have potential applications in the field of optical communications such as on-chip optical amplifiers and loss compensated devices for *Si*-photonics. However, the microstructural differences of metastable EDTS from the base silica are not completely understood, except its higher material density than silica and the superior spectroscopic characteristics [16]. Therefore, it is essential to evaluate the structural characteristics and stability of EDTS at high temperatures, which in turn could validate its compatibility with a standard CMOS manufacturing process for the imminent product developments.

In this study, the high-temperature (300 °C to 1000 °C) investigations were carried out on a representative EDTS sample ×1 of thickness 1 μm fabricated on a silica glass (spectrosil 2000) of dimensions 30 mm (L) × 20 mm (W) × 1 mm (T). The sample was prepared by the fs-laser ablation (fs laser energy 50 μJ, wavelength 800 nm, estimated laser peak intensity ~10^{13} W/cm^2, pulse width 100 fs, and pulse repetition rate 1 kHz) of a tellurite glass target of molar composition 79.5TeO_2-10ZnO-10Na_2O-0.5Er_2O_3. The structural characterization was carried out using X-ray diffraction (Philips PANalytical X'pert Diffractometer) and high-resolution transmission electron microscopy (HRTEM) (FEI Tecnai F20 200 kV FEGTEM) techniques. For the in-situ high-temperature XRD, the sample ×1 was diced into smaller dimensions of 15 mm × 15 mm to fit in the XRD stage. The sample holder attached to the hot stage was covered with a platinum foil, prior to placing the sample in, to protect the holder from any damages, in the event of glass melting at high temperatures. The sample was heated in steps from 300 °C to 1000 °C with a step size of 25 °C. At each temperature, the sample was held for 30 min and the XRD measurements were performed across the 2θ range 10–80° (scan rate: 0.05°/second). After the

* Corresponding author.
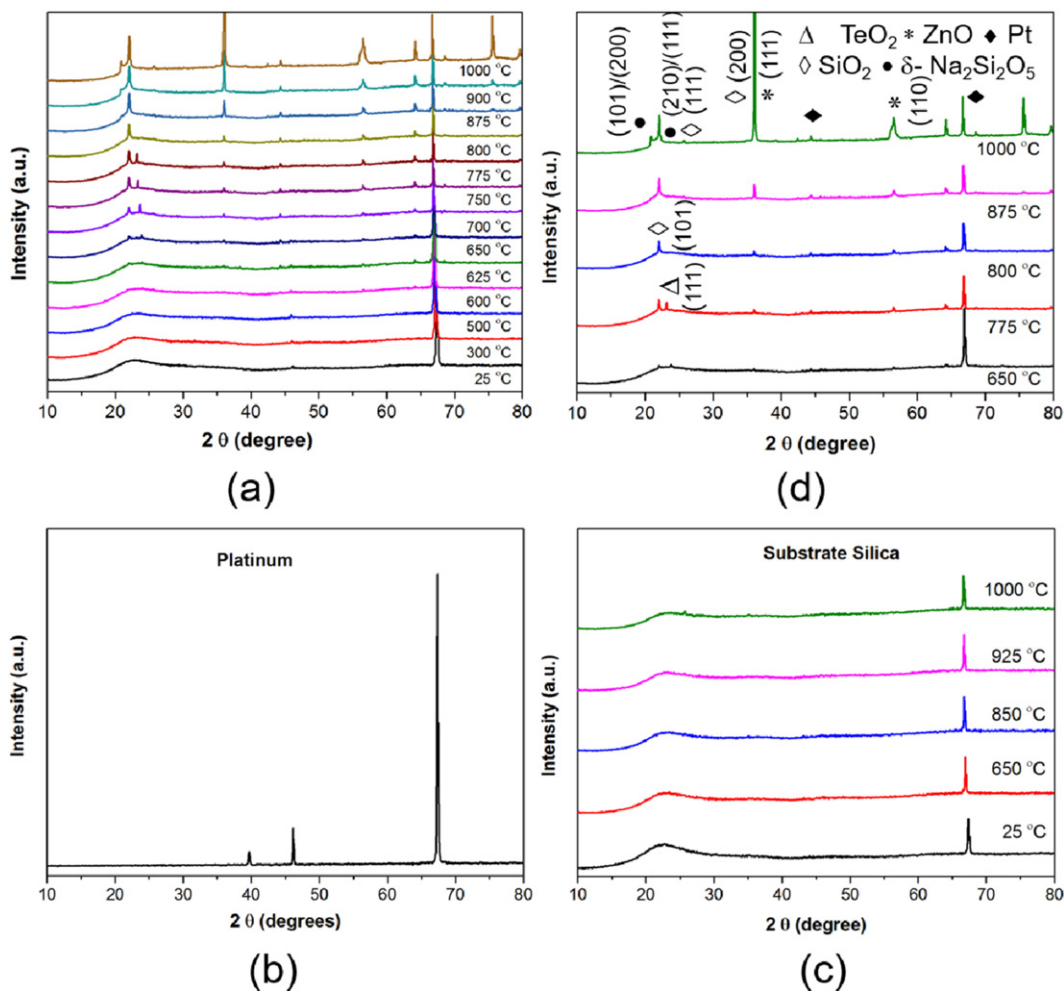E-mail address: J.Chandrappan@leeds.ac.uk (J. Chandrappan).

Fig. 1. X-ray diffraction patterns for (a) EDTS as fabricated (25 °C), and in-situ high temperature data between 300 °C and 1000 °C indicating the progressive crystalline phase development of EDTS, (b) platinum foil at room temperature, (c) substrate silica in the temperature range 25 °C to 1000 °C, and (d) selected XRD patterns of EDTS with indexing of the likely peaks corresponding to $Na_2Si_2O_5$, SiO_2, TeO_2 and ZnO in the temperature range 650 °C to 1000 °C.
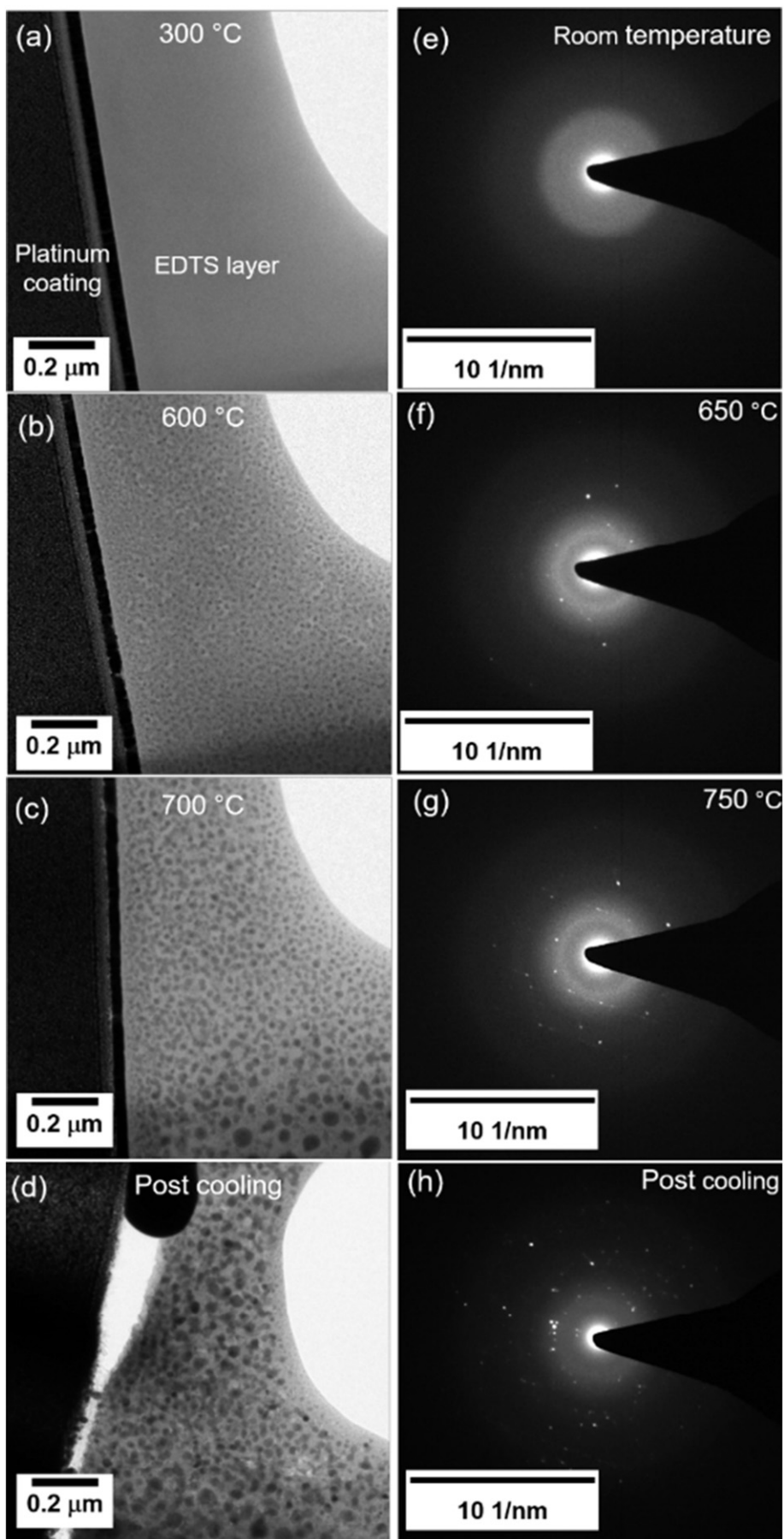
experiment, the sample was allowed to undergo a natural cooling back to the room temperature. The post-annealing XRD scan was performed to ensure that the phase change produced in the material are permanent, even after the cooling. The X'pert High Score Plus software package was used to index the peaks detected in the experimental diffraction patterns. The XRD patterns of a pure silica substrate and the platinum foil were also recorded under the same experimental conditions to authenticate the XRD peaks obtained from EDTS. For the in-situ high-temperature TEM imaging and selected area electron diffraction (SAED) analysis, a section of the sample ×1 was extracted using the standard FIB TEM sample preparation method [20] and attached to a TEM grid. This grid was subsequently examined by TEM using a Gatan Model 628 single tilt heating holder. TEM bright field images and SAED data were recorded using a Gatan Orius SC600 CCD camera. The temperature cycle used for this experiment was kept the same as that in the XRD analysis.

Prior to the high-temperature studies, the room temperature (25 °C) XRD, HRTEM images and SAED patterns were also obtained from the sample to identify the basic structure of EDTS as-fabricated. This assorted analysis confirmed the amorphous phase of EDTS. Further, the evaluations were initiated with the in-situ high-temperature XRD experiments and the patterns collected on the set temperatures are

presented in Fig. 1a. At room temperature, three peaks corresponding to the 2θ angle of 39.68°, 46.12°, and 67.38° were observed. These peaks correspond to platinum (Pt, ICDD reference code: 04-002-0887), which was confirmed by the XRD pattern collected from the platinum foil alone, as shown in Fig. 1b. The XRD pattern collected from the substrate silica glass is presented in Fig. 1c, under the same experimental conditions, which shows a low-intensity band peaked at 25.79° at 1000 °C and a stable peak at 67.38° corresponding to the background platinum foil. This analysis proved the absence of any crystals of detectable size and the amorphous phase of the base silica up to the maximum temperature employed in this study. Hence, it is asserted that all the peaks (excluding the Pt peaks) appearing in the XRD pattern presented in Fig. 1a are those characteristic of EDTS at elevated temperatures.

The absence of any significant XRD peak at room temperature validates the amorphous structure of EDTS as fabricated. It is evident from the XRD patterns that the composite material starts to lose its amorphous nature at temperatures above 600 °C. The diffraction peaks appearing with the increased temperatures from 600 °C onwards indicate the progressive crystalline phases in EDTS. However, analysing a mixture of new crystalline phases and a perfect match for all the peaks with the existing ICDD database was not practical. Therefore, the approach here was to identify the known crystal structures and

Fig. 2. HRTEM cross-sectional images and SAED patterns of EDTS captured at various temperatures presenting the evolution of crystalline phases in EDTS. HRTEM micrographs of EDTS at (a) 300 °C, (b) 600 °C, (c) 700 °C, and (d) post experiment, cooled to room temperature. Selected area diffraction pattern collected from the middle of EDTS at (e) as fabricated, (f) 650 °C, (g) 750 °C, and (h) after cooling the sample to room temperature.
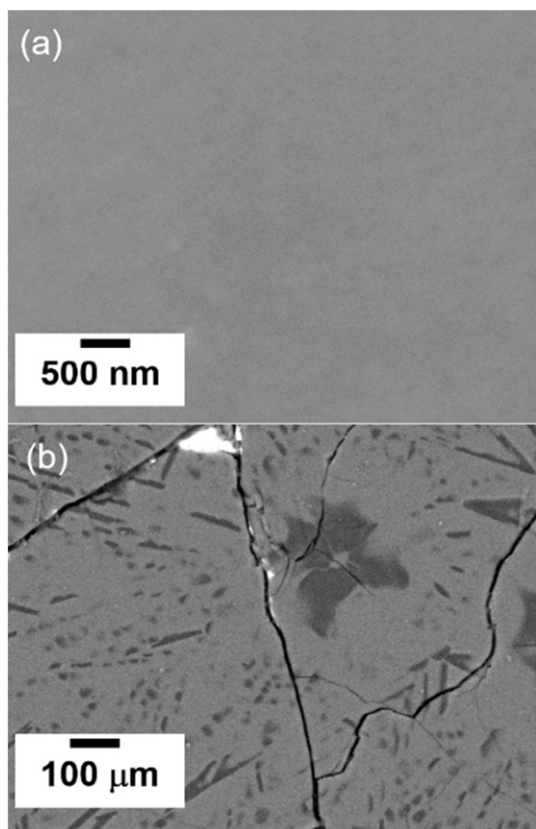
(a) 300 °C
Platinum coating
EDTS layer
0.2 μm

(b) 600 °C
0.2 μm

(c) 700 °C
0.2 μm

(d) Post cooling
0.2 μm

(e) Room temperature
10 1/nm

(f) 650 °C
10 1/nm

(g) 750 °C
10 1/nm

(h) Post cooling
10 1/nm

Fig. 3. SEM surface image of the sample ×1 (a) as fabricated, (b) after the in-situ hot stage XRD experiment.

compare them to the exact XRD patterns obtained [21]. Fig. 1d presents the XRD patterns with indexed peaks corresponding to the possible crystalline structures of $Na_2Si_2O_5$, SiO_2, TeO_2 and ZnO present in EDTS at high temperatures.

Based on the distinct peaks observed, the XRD patterns could be divided into two main regions. Significant crystalline phase developments in the diffraction pattern were observed for 2θ angles between 20° and 30° for temperatures above 600 °C, representing the formation and disappearance of different crystalline phases, whereas the crystalline phases developed above 600 °C, corresponding to the 2θ angles >30°, show no such remarkable transformations. Notably, both these regions were developed simultaneously after 600 °C as shown in Fig. 1a, but the patterns that appeared beyond $2\theta = 30°$ have only steadily growing peaks and no other distinct crystalline phase transformations are detected with the temperature rise. In contrast, the patterns observed for 2θ angle <30° are not consistent with temperature variations and unveil some interesting crystalline phase formation and disappearance at specific temperature.

The region above $2\theta = 30°$ corresponds to the stable crystalline phases that are formed where the dominant peaks correspond to ZnO and the Pt foil. The peaks at 36.11° and 56.63° match well to that of Zincite (ZnO (101) and (110)), ICDD reference code: 04-008-8199). The intensity of the diffraction peaks increased with temperature, particularly after 800 °C, which could be due to the fact that heat treatment improves the crystal growth of ZnO [22]. The peaks appearing beyond 60° 2θ, except the peak for Pt at 67.38°, were not identified.

The region $2\theta < 30°$, random crystalline phase changes are occurring between 600 °C and 900 °C. Two prominent peaks start to appear; at 22.05° and 23.82° that are indexed to Cristobalite (SiO_2 (101), ICDD reference code: 01-075-0923) and Tellurite (TeO_2 (111), ICDD reference code: 00-009-0433) respectively at 650 °C. These peaks displayed an increasing intensity with temperature indicating the possible increase in

crystallinity in the structure. With the increase in temperature, full-width half maximum (FWHM) of the SiO_2 peak at 22.05° increased. The appearance of the peak at 23.82° corresponding to TeO_2 (111) at 650 °C indicates its decomposition from the modified silica network around this temperature. The subsequent vanishing of the TeO_2 23.82° peak at 800 °C was a unique observation that brings in some interesting findings regarding the crystalline phase dynamics in EDTS. TeO_2 is volatile (heat of vaporization, 52.55 kJ/mol, is the lowest for Te among all other constituents of EDTS) and it was noticed that a considerable amount of tellurium would dissipate during the fabrication process at high temperatures [16,23]. The absence of TeO_2 peaks at 800 °C shall, therefore, be attributed to a complete evaporation of Te from the EDTS occurring at under hot conditions used in this study. At 850 °C, a new peak at $2\theta = 21.09°$ appeared corresponding to that of sodium silicon oxide (δ-$Na_2Si_2O_5$ (101)/(200)), ICDD reference code:4-009-2739) and remains stable even after cooling the sample. The strongest peak from the reference data for (δ-$Na_2Si_2O_5$ (210)/(111)) ($2\theta = 22.41°$) is weak in the XRD pattern obtained. This could be due to the overlapping by the broader and relatively intense peaks of SiO_2. It is interesting to see the formation of $Na_2Si_2O_5$, which was initiated after the complete release of Te from the EDTS. It might be possible that the absence of Te in the compound facilitated the formation of $Na_2Si_2O_5$, or it could be purely related to the temperature that supports the growth of $Na_2Si_2O_5$ from the oxides of Na and Si [24]. Remarkably, no peaks corresponding to erbium or its associated compound were observed in the analysis. The absence of an erbium compound is likely due to its lower concentrations in EDTS, or possibly, the erbium peaks are enveloped by the presence of other dominant crystalline phases in the EDTS.

The in-situ high-temperature XRD findings were further validated using the HRTEM and SAED techniques as presented in Fig. 2a–h. The HRTEM micrograph in Fig. 2a and the clear halo ring pattern in the Fig. 2e confirm the absence of any nanocrystallites or other crystalline structures in the EDTS, as fabricated. At 600 °C, the diffracted spots started to appear and it developed with temperature. This is similar to the emergence of the 23.82°/22.05° peak observed in the XRD measurements, which was clear at 625 °C. These changes demonstrate the increase in crystallinity of the EDTS with rising temperature. However, not all SAED patterns followed this trend. This could be due to the far smaller volume of the specimen analysed with SAED compared to XRD and thus only collects strong reflections if the crystallites within that small volume exist in the correct orientation with respect to the incoming beam: a fundamental limitation of SAED analysis [21]. Fig. 2b, c, d show the micrographs of the sample at high temperatures where the coherently scattering domains are uniformly distributed inside the amorphous matrix indicating the nucleation of nanocrystals. Also, these images clearly show the evolution of crystallites in EDTS with temperature, precisely matching to the XRD observations. The image collected after the cooling of the specimen to room temperature, Fig. 2d and h confirm that the decomposition and the nanocrystallites produced in the EDTS with temperature are irreversible.

All the above results reveal the crystalline phase transitions of a metastable EDTS layer on silica host glass at high temperatures, while a pure silica glass remains in the amorphous phase and does not show these crystalline transformations in the temperature range engaged in this study. Moreover, the study gave a direct observation of the EDTS structural changes from amorphous to crystalline at temperatures above 600 °C. We hypothesize that these crystallisations might be triggered by the phase separation of the EDTS and subsequent nucleation of constituents such as ZnO, SiO_2, $Na_2Si_2O_5$ and TeO_2, which in turn grew subject to the analysis temperature. The distinctive changes in the XRD, SAED pattern, and HRTEM micrographs are a clear validation of nano-crystallite formation in EDTS with increasing temperature.

The absence of TeO_2 peaks at 800 °C due to the complete evaporation of Te from the EDTS was later investigated by taking the SEM surface image and SEM-EDX of sample ×1 that underwent the in-situ hot stage XRD. The surface images of the sample before and after the heat

treatment are displayed in Fig. 3a and b respectively, which show that the thermal treatment destroyed the EDTS glassy texture and generated several cracks on the surface. The corresponding SEM-EDX did not show the intensity peaks corresponding to Te in the heat treated sample and confirmed the complete loss of Te from the EDTS at high temperatures.

In summary, we have studied the high-temperature effects on the EDTS fabricated by ultrafast laser plasma process and shown that EDTS is thermally stable at temperatures below 600 °C. This leads to the conclusion that EDTS could very well integrate with the *Si*-photonics manufacturing process, such as a CMOS back-end-of-line process (<500 °C). Additionally, the optical performance of a device fabricated on EDTS will not be affected by the highest rated operating temperature of 85 °C. The dynamics of amorphous to crystalline phase transformation of EDTS with temperature might be more complex than hypothesized here. Further studies are proposed to estimate the coordination number of individual ions and morphology of EDTS, which would shed more light on the reaction kinetics associated with the devitrification.

References

[1] W.J. Miniscalco, J. Lightwave Technol. 9 (1991) 234–250.
[2] A. KENYON, Prog. Quantum Electron. 26 (2002) 225–284.
[3] G.C. Righini, M. Ferrari, Riv. DEL NUOVO Cim. 28 (2006) 1–53.
[4] M.J.F. Digonnet, Rare Earth Doped Fiber Lasers and Amplifiers, Marcel Dekker, 1993.
[5] A. Polman, J. Appl. Phys. 82 (1997) 1.
[6] A. Polman, in: S. Jiang (Ed.), SPIE 3942 2000, pp. 2–13.
[7] S. Serna, W. Zhang, X. Leroux, D. Gao, D. Zhang, L. Vivien, E. Cassan, J. Opt. Soc. Am. B 31 (2014) 2021.
[8] E. Snoeks, P.G. Kik, A. Polman, Opt. Mater. (Amst) 5 (1996) 159–167.
[9] A. Polman, J.S. Custer, P.M. Zagwijn, a.M. Molenbroek, P.F.a. Alkemade, J. Appl. Phys. 81 (1997) 150.
[10] H. Isshiki, F. Jing, T. Sato, T. Nakajima, T. Kimura, Photosynth. Res. 2 (2014) A45.
[11] Y. Arakawa, T. Nakamura, Y. Urino, T. Fujita, IEEE Commun. Mag. 51 (2013) 72–77.
[12] X. Chen, C. Li, H.K. Tsang, NPG Asia Mater. 3 (2011) 34–40.
[13] M.J.R. Heck, J.F. Bauters, M.L. Davenport, J.K. Doylend, S. Jain, G. Kurczveil, S. Srinivasan, J.E. Bowers, IEEE J. Sel. Top. Quantum Electron. 19 (2013) 6100117.
[14] R. Soref, IEEE J. Sel. Top. Quantum Electron. 12 (2006) 1678–1687.
[15] S. Fathpour, Nanophotonics 4 (2015) 143–164.
[16] J. Chandrappan, M. Murray, T. Kakkar, P. Petrik, E. Agocs, Z. Zolnai, D.P. Steenson, A. Jha, G. Jose, Sci. Rep. 5 (2015) 14037.
[17] G. Jose, T.T. Fernandez, D. Steenson, A. Jha, Conf. Lasers Electro-Optics 2012, 2012 (CM3L.6).
[18] J. Chandrappan, M. Murray, P. Petrik, E. Agocs, Z. Zolnai, A. Tempez, S. Legendre, D.P. Steenson, A. Jha, G. Jose, Opt. Mater. Express 5 (2015) 2849.
[19] K.C. Phillips, H.H. Gandhi, E. Mazur, S.K. Sundaram, Adv. Opt. Photon. 7 (2015) 684–712.
[20] L.A. Giannuzzi, F.A. Stevie, Micron 30 (1999) 197–204.
[21] B. Fultz, J. Howe, Transmission Electron Microscopy and Diffractometry of Materials, Springer Berlin Heidelberg, Berlin, Heidelberg, 2013.
[22] K.J. Chen, T.H. Fang, F.Y. Hung, L.W. Ji, S.J. Chang, S.J. Young, Y.J. Hsiao, Appl. Surf. Sci. 254 (2008) 5791–5795.
[23] P. Balling, J. Schou, Rep. Prog. Phys. 76 (2013) 36502.
[24] A.I. Zaitsev, Z.V. Dobrokhotova, A.D. Litvina, B.M. Mogutnov, J. Chem. Soc. Faraday Trans. 91 (1995) 703.